FERMILAB-PUB-75-153-E
Submitted to
Nuclear Physics B
July 1975

INELASTIC 2-PRONG EVENTS IN 147 GeV/c $\pi^- p$ COLLISIONS*

D. Fong, M. Heller, A. Shapiro, M. Widgoff
Brown University, Providence, Rhode Island 02912

F. Bruyant
CERN, Geneve 23, Switzerland

D. Bogert, M. Johnson
Fermilab, Batavia, Illinois 60510

R. Burnstein, C. Fu, D. Petersen, M. Robertson, H. Rubin
Illinois Institute of Technology, Chicago, Illinois 60616

R. Sard, A. Snyder, J. Tortora
University of Illinois, Urbana, Illinois 61801

D. Alyea
Indiana University, Bloomington, Indiana 47401

C-Y Chien, P. Lucas, A. Pevsner, R. Zdanis
Johns Hopkins University, Baltimore, Maryland 21218

J. Brau*1, J. Grunhaus*2, E.S. Hafen, R.I. Hulsizer, U. Karshon*3
V. Kistiakowsky, A. Levy*4, A. Napier, I.A. Pless, P.C. Trepagnier,
J. Wolfson, R.K. Yamamoto
Massachusetts Institute of Technology, Cambridge, Massachusetts 02139

H. Cohn
Oak Ridge National Laboratory, Oak Ridge, Tennessee 37830

T.C. Ou, R. Plano, T. Watts
Rutgers University, New Brunswick, New Jersey 08903

E. Brucker, E. Koller, P. Stamer, S. Taylor
Stevens Institute of Technology, Hoboken, New Jersey 07030

W. Bugg, G. Condo, T. Handler, E. Hart
University of Tennessee, Knoxville, Tennessee 37916

H. Kraybill, D. Ljung, T. Ludlam, H.D. Taft
Yale University, New Haven, Connecticut 06520

ABSTRACT

The Proportional Wire Hybrid System at the Fermilab 30-in. bubble chamber is employed to isolate and analyze the inelastic 2-prong events in $\pi^- p$ collisions at 147 GeV/c. These result mainly from diffractive processes. Beam and target excitation contribute with nearly equal cross sections. A double diffractive component is indicated with roughly the cross section predicted on the basis of simple factorization arguments. The non-diffractive component ($\sim$20%) exhibits behavior characteristic of particle production in many-body final states. No conclusive evidence is seen for a double Pomeranchuk exchange process, although a small contribution from this mechanism cannot be ruled out.

*This work supported in part by the U.S. Energy Research and Development Administration and the National Science Foundation.

*1Fannie and John Hertz Foundation Fellow

*2On leave of absence, Tel-Aviv University, Israel

*3On leave of absence, The Weizmann Institute of Science, Israel

*4Present address, Tel-Aviv University, Israel

I. Introduction

An important result of high energy hadron collision experiments has been the identification of some 15-20% of the inelastic cross section with quasi-elastic scattering: diffractive excitation of the beam or target particle. This process contributes mainly to final states of small charged-particle multiplicity, and has been accessible to study in bubble chamber experiments primarily as a characteristic low-mass peak in the spectrum of missing mass recoiling from a slow proton in the laboratory frame. While such processes are known to be the major contribution to inelastic 2-prong events, investigation of these channels is hampered by the difficulty of separating elastic from inelastic events, and by the fact that much of the information for each event is carried by neutral particles which go unobserved.

In a recent paper[1] we presented first results from a study of 147 GeV/c $\pi^- p$ collisions in the Fermilab 30-in. bubble chamber utilizing external proportional wire planes to obtain good momentum resolution for fast secondary tracks. With this Proportional Wire Hybrid System (PWHS) a clean separation of elastic and inelastic 2-prongs is obtained on an event-by-event basis. We find (Ref. 1) that quasi-elastic processes account for some 70% of the 2-prong inelastic events, and factorization arguments may be used to infer that ∿80% of the 2-prong inelastic cross section results from diffractive processes.

In this paper we present a detailed analysis of the inelastic 2-prong events, studying the reactions

$$\pi^- p \to \pi^- p + \text{neutrals} \qquad (1)$$

$$\pi^- p \to \pi^- \pi^+ + \text{neutrals} \qquad (2)$$

In Sec. II we discuss some features of the experiment, including the separation of elastic from inelastic events and the identification of events corresponding to Reactions 1 and 2. In Sec. III we show that even though there are unseen neutrals in each event, a simple kinematic classification based on the measured variables of the charged tracks serves to isolate the contributions from specific production mechanisms with very little ambiguity or background. This classification is substantiated by the data obtained from a forward γ-ray detector placed downstream of the hybrid spectrometer. The characteristic features of few-body, diffractive processes are readily discerned, as is a non-diffractive component for which the behavior of the observed particles is similar to that of pairs of particles produced in high-multiplicity final states.

In Sec. IV we analyze each of these processes in turn and calculate cross sections. A summary and discussion of the results is given in Sec. V.

II. Experiment and Data Sample

The Proportional Wire Hybrid System is diagrammed in Fig. 1. It consists of the Fermilab 30-in. bubble chamber with an array of proportional wire chambers (PWC's) both upstream and downstream[1]. The trajectory of each incident beam track is determined by the upstream array, which includes a Cerenkov counter for mass tagging. The trajectories of fast tracks exiting the downstream window of the bubble chamber are determined by chambers D, E, F, and G. Chamber H, which is preceded by 2.5 radiation lengths of lead, is used to detect the presence of fast forward γ-rays.

The data for each event consists of the bubble chamber images on film (three views) plus the proportional wire readout, which is stored sequentially for each incident beam track in each spill. No triggering is required, and no event preselection is performed.

Each event is reconstructed from the film measurements (obtained with the automatic measuring device PEPR) and the PWC information, using a sequence of computer programs especially written for the PWHS. Essentially, all tracks with laboratory momentum greater than 15 GeV/c traverse the downstream wire planes, and for these the additional magnetic path length of the bubble chamber fringe field affords particle momentum measurements with substantially greater precision than can be obtained from the bubble chamber alone. For fast secondary tracks originating inside the bubble chamber, the error on momentum is given by $\Delta p/p \simeq \pm .0006\ p$, with p in units of GeV/c. With an incident beam momentum of 150 GeV the momentum of each outgoing track is determined with an accuracy of $\pm$ 10% or better.

The data for the present experiment consists of 105,000

pictures obtained in an exposure of the PWHS to a beam of 147 GeV/c π^- mesons. All of the interactions within a specified fiducial volume have been scanned, measured and reconstructed as described above, yielding a sample of 1640 2-prong events for analysis. A second scan of the film has been performed for cross section determinations, and all 2-prong events for which the initial reconstruction was deemed unsatisfactory have been remeasured using manually operated measuring devices.

Two techniques were employed for separating elastic from inelastic 2-prongs. As described in Ref. 1, an accurate identification of elastic events is obtained by using the measured momentum of the slow recoil proton to predict the trajectory of the outgoing pion as it traverses the downstream proportional wire planes. The predicted and observed trajectories are then compared, with a spatial resolution of . 5 mm and an angular resolution of .1 mr in the downstream counters. As a second technique, all 2-prong events were fit to the four-constraint elastic hypothesis using the kinematic fitting program SQUAW. The results of the two procedures were found to be in excellent agreement: Differences at the few-percent level resulted from border effects in the selection of cut-off criteria. For the analysis which follows, in order to minimize background in the inelastic sample, an event was assigned to the elastic channel if it was called elastic by either technique. Approximately 5% of the two-prong events have a fast outgoing negative track which scatters either in the liquid hydrogen or in the exit window of the bubble chamber and is lost to the downstream system. For these events the results of the SQUAW fit to the bubble chamber

measurements were accepted in making the elastic/inelastic assignment.

As a result of this separation, 1019 events were assigned to the elastic channel leaving an inelastic sample of 621 events. We estimate that the background in the inelastic sample due to mis-assigned elastics is at most 20-30 events (<5%) with a similar upper limit for the number of inelastic events wrongly assigned to the elastic channel. The elastic and inelastic signals, as seen in the spectra of missing mass recoiling from identified protons and from the proton-π^- system, are shown in Figs. 2 and 3.

After correcting for scanning losses, including a systematic bias against events with small momentum transfer to the proton, we find the elastic cross section to be 3.24±.15 mb and the cross section for inelastic 2-prongs to be 1.82±.10 mb. (A more complete discussion of the cross section determination is given in Ref. 2.) For the remainder of this paper we devote our attention to the inelastic sample. The elastic channel is treated in Ref. 2.

In classifying the inelastic 2-prongs, we assume that all positive tracks are either pions or protons*. The ionization for each track was determined from PEPR measurements of the bubble

---

*We find a cross section of 101±41 μb for K^o_s in the 2-prong sample. If it is assumed that the number of charged kaons is equal to the number of neutral kaons, then among those charged tracks which are neither protons nor leading π^- the K-meson fraction is about 10%.

density in each of the three measured views;[3] this information allows identification of protons with lab momenta up to 1.4 GeV/c. Of the 621 events in the inelastic 2-prong sample, 331 have an identified proton and are assigned to Reaction 1. The 290 remaining events are assigned to Reaction 2. The distribution in laboratory momenta for the identified protons (not shown) goes rapidly to zero at the cut-off momentum. Since the efficiency for proton identification is nearly flat up to this cut-off, we conclude that few, if any, protons are present with higher momenta.

After correcting for scanning losses and systematic inefficiencies in proton identification, the cross sections for Reactions 1 and 2 are found to be 1.10±.09 mb and 0.72±.06 mb, respectively. These results are summarized in Table 1.

III. Classification of Events

Figure 4 displays a plot of $x(\pi^-)$ vs. $x(p)$ for Reaction 1, where x denotes the scaled longitudinal momentum variable: $x = 2\,P_L^{cm}/\sqrt{s}$. The data points lie mainly in two bands, one near $x(p) = -1$ (leading proton) and another near $x(\pi^-) = +1$ (leading pion). These bands are suggestive of diffractive excitation of the beam and target, respectively, and appear to be almost devoid of background. The width of the leading pion band is consistent with the momentum resolution for fast, beam-like pions.

For comparison, we show in Fig. 5 similar plots for 4- and 6-prong events in which a proton has been identified. Here the x variable for the fastest π^- in each event is plotted against x of the proton. The leading particle bands are clearly evident in the 4-prong events, but are essentially absent in the 6-prongs. Both of these data samples are also populated by events characteristic of high multiplicity, non-diffractive final states, with relatively fast protons in the laboratory frame and pion momenta near zero in the c.m. frame. Some of this behavior is seen for the 2-prongs in Fig. 4, but here the diffractive processes clearly dominate.

The data for Reaction 2 are shown in Fig. 6, where $x(\pi^-)$ is plotted vs. $x(\pi^+)$. Again the leading pion signal is clearly distinguished, as is a concentration of events for which $x(\pi^-) \approx x(\pi^+) \approx 0$. These same data are shown in Fig. 7, in which $x(\pi^-)$ is plotted against the invariant mass of the $\pi^+\pi^-$ combination. The leading pion events are seen to be associated mainly with large values of this invariant mass, as expected for diffractive

excitation of the target proton. The events for which the observed pions appear near $x = 0$ have invariant masses which are concentrated at near-threshold values.

Thus, despite the fact that in each event one or more neutral particles go unobserved, the measured variables for the inelastic 2-prong events clearly exhibit a few special kinematic configurations corresponding to local concentrations of events in the many-dimensional phase space volume. To facilitate a quantitative discussion, we divide each of Reactions 1 and 2 into three kinematic regions, indicated by the dashed lines in Fig. 4,6, and 7:

Reaction 1 -	Region i	: $x(p) \leq -.95$
	Region ii	: $x(p) > -.95$, $x(\pi^-) > 0.76$
	Region iii	: $x(p) > -.95$, $x(\pi^-) \leq 0.76$
Reaction 2 -	Region i	: $x(\pi^-) > 0.76$
	Region ii	: $0.18 < x(\pi^-) \leq 0.76$
	Region iii	: $x(\pi^-) \leq 0.18$

In each of these regions the behavior of the charged particles is indicative of specific dynamical processes, with apparently very little overlap of the contributing production mechanisms from region to region. The behavior of the fast neutral particles is consistent with this observation, as illustrated in Fig. 8. Here, for a subsample of about 1/3 the data, the intensity of electromagnetic energy impinging on counter H (Fig. 1) is

histogrammed for each of the 6 kinematic regions*. A high degree of correlation between the neutral particle and charged particle behavior is evident. As expected, events with leading, beam-like pions are not accompanied by fast γ rays. Events with a leading proton are almost always accompanied by some electromagnetic energy incident on the lead converter, with the majority of these events having maximum intensity on our scale of 0-6. Events with neither a leading pion nor a leading proton are divided between large and small intensities of forward electromagnetic radiation.

In the following Section we exploit this kinematic classification as a means for isolating particular mechanisms for particle production; specifically: diffractive excitation of the beam or target, double-diffractive excitation, and non-diffractive processes characteristic of many-body final states.

---

*Counter H subtends an angle of $\pm 1.5°$ at the bubble chamber center and consists of 156 wires in three PWC planes. We obtain a rough measure of the intensity of electromagnetic energy impinging on the lead converter by counting the number of fired wires. We have arbitrarily set the intensity scale from 0 to 6, where 0 indicates no fired wires and 6 indicates more than 100 fired wires.

IV. Analysis and Cross Sections

A. Projectile Excitation

The component of the inelastic 2-prong sample which is due to single diffractive excitation of the incident π^- can only appear in Reaction 1. As noted above, this signal is clearly seen in Fig. 4, and the boundary for Region i on this plot was chosen to isolate this process. The cut-off at $x(p) = -.95$ corresponds to a squared missing mass recoiling from the proton of about 14 GeV^2 (See Fig. 2b).

The distribution in momentum transfer from the target to the outgoing proton for these events is shown in Fig. 9a. The apparent dip in the forward direction can be accounted for by scanning losses due to very short recoil proton tracks. For larger values of t the fall-off is consistent with exponential. The best-fit slope in the region $.05 < |t| < .45$ $(GeV/c)^2$ is $10.1 \pm .7$ $(GeV/c)^{-2}$. This is to be compared with a slope of $8.3 \pm .5$ obtained for the elastic differential cross section in this experiment[2] over a similar range of t.

Fig. 9b shows the invariant mass distribution of the proton and π^- for these events. Although the spectrum extends from near-threshold up to the kinematic limit, the tendency is toward large values of this invariant mass, with no evidence for low-mass resonances. (Since we have here selected protons of very limited momenta, this mass spectrum largely reflects the π^- momentum distribution.)

In Fig. 9c is shown the distribution in the azimuthal correlation angle, ϕ, defined by the relation:

$$\cos \Phi = \hat{p}_T(p) \cdot \hat{p}_T(\pi) \quad ,$$

where $\hat{p}_T$ for each track is the unit vector along the direction of the transverse momentum. A strong correlation is observed, with the most probable configuration being that in which the proton and π^- are aligned back-to-back in the transverse plane.

All of these features are characteristic of few-body, diffractive excitation processes, and we attribute all of the events in Reaction 1, Region i to diffractive excitation of the incident π^-. We note that the band of events populating this region in Fig. 4 exhibits some structure. The concentration of points near $x(\pi^-) = 0$, and the broad enhancement between $x = .6$ and .8 are readily reproduced by very simple models for the production of a low-mass, diffractively excited object which decays to a vector meson plus a pion (e.g., $A_1^- \to \rho^-\pi^\circ$). The small enhancement seen near $x(\pi^-) = .3$ is not so readily understood, and is currently the subject of more detailed investigation.

All of the events in Reaction 1, Region i contain leading protons ($x(p) \simeq -1$). Some of these events also contain leading π^-, i.e., the band of events in this region of Fig. 4 extends to $x(\pi^-)$ near +1. Although this behavior is not inconsistent with the mechanism discussed above, it is worth scrutinizing these "double-leading" (DL) events in terms of the double-Pomeranchuk exchange (DPE) diagram illustrated in Fig. 9d. It has been suggested that this process, where X° in Fig. 9d is mainly $\pi^\circ\pi^\circ$, might contribute with a cross section of about 10 μb in this energy range[4], which would correspond to ∿3 events in our data sample. If the Pomeranchuk singularity is a simple pole, we expect the DPE contribution to be isotropic in the azimuthal angle ϕ[4,5]. In Fig. 9c the shaded events are those for which

$x(\pi^-) > .76$. The number of DL events is almost an order of magnitude higher than predicted for the DPE case, and their distribution is not isotropic, but rather shows the same backward peaking which characterizes the whole of the band of events in Region i. We conclude that the bulk of the DL events in the 2-prong sample are not associated with the DPE mechanism. However the ϕ distribution of Fig. 9c (shaded) is not inconsistent with a contribution from DPE as predicted in Ref. 6.

Our estimate for the cross section for diffractive excitation of the pion projectile, in the 2-prong sample, is obtained by calculating the cross section for events in Reaction 1, Region i, correcting for small-t losses. The result is $.65 \pm .06$ mb (see Table II).

B. Target Excitation

Events which have a leading π^- meson, and are not associated with the leading proton signal, appear in Region ii of Reaction 1 (Fig. 4) and Region i of Reaction 2 (Figs. 6,7). For these events the distributions in momentum transfer from the incident to the outgoing π^- are shown in Fig. 10a, b. For both of Reactions 1 and 2 these differential cross sections are well described by an exponential form. Within the limits of statistical accuracy the two exponential slopes are identical, and consistent with the elastic slope. The distributions in ϕ, the azimuthal correlation angle between the transverse momentum vectors of the observed π^- and proton for Reaction 1, and π^- and π^+ for Reaction 2, are shown in Fig. 10d,e. In both cases the high degree of correlation expected for few-body diffractive excitation

processes is observed (c.f. Fig. 9c). We conclude that both samples of events correspond to the production of diffractively excited nucleon states whose decay products may include a proton (Reaction 1) or a neutron (Reaction 2). The summed momentum transfer distribution, including both leading pion samples, is shown in Fig. 10c. An excellent fit to an exponential dependence is obtained, yielding a slope of 8.4 ± 1.1 $(\mathrm{GeV.c})^{-2}$. There is no evidence for non-diffractive background.

After correcting for scan losses and wrongly identified protons (as discussed in Sec. II), we obtain a cross section of $.72 \pm .05$ mb for diffractive excitation of the target proton. Of this, $.31 \pm .03$ mb is due to Reaction 1 (Region ii) and $.41 \pm .04$ mb corresponds to Reaction 2 (Region i).

C. Double Diffractive Excitation

Single diffractive excitation of the beam or target, as discussed in the preceding paragraphs, accounts for ~75% of the inelastic 2-prongs. The total diffractive contribution, illustrated schematically in Fig. 11, presumably includes double-diffractive processes (Fig. 11d,e). If it is assumed that the cross sections for diffractive excitation of the beam or target particle result from the same exchange mechanism which mediates elastic scattering (i.e., Pomeranchuk exchange) and, further, that the amplitudes may be factorized into a part which depends only on the pion vertex and a part which depends only on the proton vertex, then the expected cross sections for double-diffractive excitation (DD) in the 2-prong events may be written as follows:

$$\sigma_{DD}^{(2)} = \frac{\sigma_{\pi^* p}^{(2)} \quad \sigma_{\pi p^*}^{(2)}}{\sigma_{el}} \quad . \tag{3}$$

Here $\sigma_{\pi^* p}$ ($\sigma_{\pi p^*}$) are the cross sections for single excitation of the beam (target). All of the cross sections in equation 3 are for 2-prong events*. Substituting the cross sections obtained above for beam and target excitation we calculate $\sigma_{DD}^{(2)}$ = .144 ± .020 mb of which .054 ± .011 mb appears in Reaction 1 (events with a proton in the final state), and .086 ± .016 mb in Reaction 2.

We may now ask whether these results are consistent with the data. For these 2-prong events the diffractively produced objects have masses of the order of 3 GeV or less: For pion excitation this can be seen directly form the width of the leading proton band in Fig. 4. For the leading pions the resolution width allows the possibility of larger masses, but we expect, on the basis of constrained fits in the 4-prong events and the results of p-p scattering at high energies[6] that this is not the case.

---

*With our assumptions, Equation 3 is strictly true for differential cross sections at fixed t. The integrated relation holds if the elastic and single diffractive amplitudes have the same dependence on momentum transfer. This is found to be the case for the data under consideration here (Sec. IV A,B).

For such low-mass excited objects, it may be verified that at the energy of this experiment the cm momentum spectrum of the π^- fragment of the beam is very nearly independent of whether or not the target proton is excited in the collision. Then for the double-diffractive events we expect the π^- spectrum to have the same shape as that observed in Region i of Fig. 4. Thus, by normalizing the observed π^- spectrum for leading proton events in Reaction 1 to the cross section $\sigma_{DD}^{(2)}$ we obtain a prediction, based on the factorization assumptions, for the distribution of π^- from double-diffractive events.

This prediction is shown as the broken histogram in Fig. 12. Here the solid histogram is the distribution of π^- for Reactions 1 and 2 after removing the leading proton events. The events in the peak with $x \gtrsim .76$ correspond to target excitation (Fig. 11b,c) and events with $x < .18$ mostly result from non-diffractive processes (see Sec. IV D, below). The factorization prediction for the shape of this distribution at intermediate values of x falls below the data by about a factor of two in normalization. While this is by no means a demonstration that a double diffractive component is present in the amount predicted on the basis of factorization, it does indicate that a substantial fraction of the events in Region iii of Reaction 1 and Region ii of Reaction 2 may result from such a mechanism. If we are indeed observing double diffractive excitation, there must be at least five particles in the final state, with the π^- associated with beam break-up, and the π^+ or proton a fragment of the target. For this case we expect little correlation in ϕ between the two observed particles. This expectation is borne out, as seen in Fig. 13a, b.

D. Non-Diffractive Processes

A significant fraction of the π^- mesons produced in the 2-prong events occur in a peak near $x = 0$ (Fig. 12). These cannot all be accounted for by diffractive processes, at least insofar as we have employed the factorization hypothesis to estimate the double diffractive contribution. For Reaction 2 these events, which lie in Region iii of Figs. 6 and 7, have both the π^+ and π^- near $x = 0$. The effective mass distribution for the two charged pions is confined to very small values, rising sharply from threshold, and is peaked below the ρ mass (Fig. 13d). The distribution in the azimuthal correlation angle shows a small asymmetry (Fig. 13c). This behavior is characteristic of centrally produced pions in many-body final states. The comparison curves shown in Fig. 13c, d are a smoothed representation of data obtained in this experiment for $\pi^+\pi^-$ pairs in 6-prong events, and clearly lend support to this observation.

For both Reactions 1 and 2 there are some events for which the π^- moves backward in the c.m. frame. These events are shown shaded in the plots of Fig. 13. Their behavior is not qualitatively different from other events with slow pions in the c.m. frame and we do not attribute them to a significant component of few-body charge exchange processes.

We conclude that the non-diffractive events seen in the 2-prong sample involve many pions centrally produced, very likely by the same mechanisms which dominate pion production in final states of higher charged particle multiplicity. The cross sections for the non-diffractive component entered in Table II are simply the difference between the total 2-prong inelastic cross sections and the diffractive cross sections obtained above.

V. Summary and Conclusions

Using a Proportional Wire Hybrid Bubble Chamber System, we have isolated the inelastic 2-prong events in $\pi^- p$ collisions at 147 GeV/c incident momentum. These events are found to be predominantly the result of diffractive (quasi-elastic) processes, with beam and target excitation contributing in equal amounts. Information from a downstream γ-ray detector has been used to assist in interpreting the kinematic behavior of the charged particles seen in the bubble chamber, although a simple classification scheme in terms of the configuration of the observed charged particles serves to separate diffractive from non-diffractive events with very little ambiguity. A double diffractive component predicted by simple factorization arguments can be acccunted for by the data. The total contribution to the inelastic 2-prongs from diffractive processes amounts to 80% of the events (1.5 mb).

Cross sections are summarized in Tables I and II. The non-diffractive component, though small, is clearly seen. For these events the observed particles exhibit behavior similar to that of pairs of particles centrally produced in many-body final states. We find no significant evidence for few-body charge exchange processes.

No compelling evidence is found for double Pomeranchuk exchange in the 2-prong data. The events in which a final-state pion and proton are both observed to be highly peripheral can be accounted for in terms of a single diffractive mechanism, and do not exhibit the azimuthal decoupling expected for the double exchange process in which the Pomeranchuk singularity is a

simple pole. Nonetheless the presence of such a component, in the small amount predicted in Ref. 4 cannot be ruled out.

We thank the data reduction personnel of the participating institutions and the staff of the MIT PEPR system for making this work possible, and we acknowledge the excellent efforts of the Fermilab Neutrino Section and 30-inch bubble chamber staffs in obtaining this exposure.

References and Footnotes

1. D. Fong et al., Phys. Letters 53B, 290 (1974)

2. Total, Elastic and Topological Cross Sections for 147 GeV/c $\pi^- p$ and $K^- p$ Collisions, PHS Consortium (in preparation)

3. PHS Internal Report no. 31, D. Ljung, Yale Univ. (Oct., 1974)

4. D.M. Chew and G.F. Chew, Phys. Letters 53B, 191 (1974)

5. D.Z. Freedman et al., Phys. Rev. Letters 26, 1197 (1971)

6. For a discussion of inelastic 2-prong events in 200 GeV/c pp collisions see S. Barish et al., Phys. Rev. D9, 1171 (1974)

Figure Captions

1. Schematic diagram of the 30-in. PWC Hybrid Bubble Chamber System, showing the location of counters upstream and downstream of the bubble chamber. The trajectories of particles in a typical 2-prong event are superimposed on the diagram.
2. The distribution of invariant mass squared recoiling from the proton. (a) Elastic events. (b) Inelastic events assigned to Reaction 1.
3. The distribution of invariant mass squared recoiling from the proton and π^-. (a) Elastic events. (b) Inelastic events assigned to Reaction 1.
4. $x(\pi^-)$ vs. x(proton) for Reaction 1. The dashed lines delineate the kinematic regions defined in the text.
5. $x(\pi_f^-)$ vs. x(proton) for (a) 4-prong events and (b) 6-prong events. Protons are identified by ionization. There is one entry per event, with π_f^- being the negative track with the largest value of center-of-mass longitudinal momentum in each event.
6. $x(\pi^-)$ vs. $x(\pi^+)$ for Reaction 2. The dashed lines delineate the kinematic regions defined in the text.
7. $x(\pi^-)$ vs. $M(\pi^+\pi^-)$ for Reaction 2. The dashed lines delineate the kinematic regions defined in the text.
8. The intensity of forward electromagnetic radiation, as detected by the H chamber, for a subsample of events in each of the 6 kinematic regions discussed in the text. The horizontal scale is arbitrary, with zero representing no counts in chamber H, and 6 representing the case where more

8. than 1/3 of the wires are fired in chamber H. (a), (b), (c): Reaction 1, Regions i, ii, iii. (d), (e), (f): Reaction 2, Regions i, ii, iii.

9. For the reaction $\pi^- p \to \pi^- p$ + neutrals; events with $x(p) < -.95$: (a) The distribution in momentum transfer from the initial to final proton. The solid line is the result of a fit to the form $d\sigma/dt = a \exp(bt)$. (b) The proton-π^- effective mass distribution. (c) The distribution in azimuth angle between the proton and π^- momentum vectors. The shaded area is the result for events with $x(p) < -.95$ and $x(\pi^-) > .76$. (d) Diagram illustrating double Pomeranchuk exchange.

10. (a) The distribution in momentum transfer from initial to final $\pi^-(d\sigma/dt_{\pi\pi})$ for the reaction $\pi^- p \to \pi^- p$ + neutrals; events with $x(\text{proton}) > -.95$ and $x(\pi^-) > .76$. The dashed line is the elastic differential cross section normalized to the plotted data. (b) $d\sigma/dt_{\pi\pi}$ for the reaction $\pi^- p \to \pi^- \pi^+$ + neutrals; events with $x(\pi^-) > .76$. The dashed line is the elastic differential cross section normalized to the plotted data. (c) The sum of the distributions in (a) and (b). The solid line is the result of a fit to the form $d\sigma/dt = a \exp(bt)$. (d) The distribution in azimuth angle between the proton and π^- momentum vectors for the reaction $\pi^- p \to \pi^- p$ + neutrals; events with $x(\text{proton}) > -.95$, $x(\pi^-) > .76$. (e) Azimuth angle distribution for the reaction $\pi^- p \to \pi^- \pi^+$ + neutrals; events with $x(\pi^-) > .76$.

11. Diagrams illustrating diffractive processes contributing to the inelastic 2-prong sample.

12. The distribution in $x(\pi^-)$ for reactions 1 and 2, with the

12. contribution from projectile excitation (Reaction 1, Region i) removed. The broken histogram is the prediction, based on the factorization hypothesis, of the double-diffractive component (see text). The dashed lines at $x = .18$, $x = .76$, indicate boundaries of the kinematic regions defined in the text.

13. (a) The distribution in azimuth angle between the proton and π^- momentum vectors for Reaction 1, Region iii. The shaded area is the contribution from events with $x(\pi^-) < 0$. (b) Azimuth angle distribution for Reaction 2, Region ii. (c) Azimuth angle distribution for Reaction 2, Region iii. The shaded area is the contribution from events with $x(\pi^-) < 0$. The smooth curve is the same distribution for $\pi^+\pi^-$ pairs in events with 6 charged prongs ($x(\pi^-) < .18$), normalized to the number of entries in the histogram. (d) The $\pi^+\pi^-$ effective mass distribution for Reaction 2, Region iii. The smooth curve, normalized to the 2-prong data, is the same distribution for $\pi^+\pi^-$ pairs in 6-prong events ($x(\pi^-) < .18$).

Table I

Two-Prong Cross Sections

Reaction	No. Events*	Cross Section (mb)
$\pi^- p \to$ 2-prongs	1640	5.06±.15
$\pi^- p \to \pi^- p$(elastic)	1019	3.24±.15
$\pi^- p \to \pi^- p$ + neutrals	331	1.10±.09
$\pi^- p \to \pi^- \pi^+$ + neutrals	290	0.72±.06
Total 2-pr inelastic	621	1.82±.10

*Listed here are the actual numbers of events assigned to each category in the 2-prong data sample. The corrections applied to obtain cross sections are discussed in the text.

Table II

Cross Sections (in millibarns) for Two-Prong Inelastic Production Mechanisms

147 GeV/c $\pi^- p$ Collisions

	$\pi^- p$+neutrals	$\pi^- \pi^+$+neutrals	Totals
Pion diffractive excitation:	.65±.06	----	.65±.06
Proton diffractive excitation:	.31±.03	.41±.04	.72±.05
Double diffractive:*	.05±.01	.09±.02	.14+.02
Non-diffractive:	.09±.02	.22±.04	.31±.05

*Calculated from the single-diffractive and elastic cross sections using the factorization hypothesis (see text).

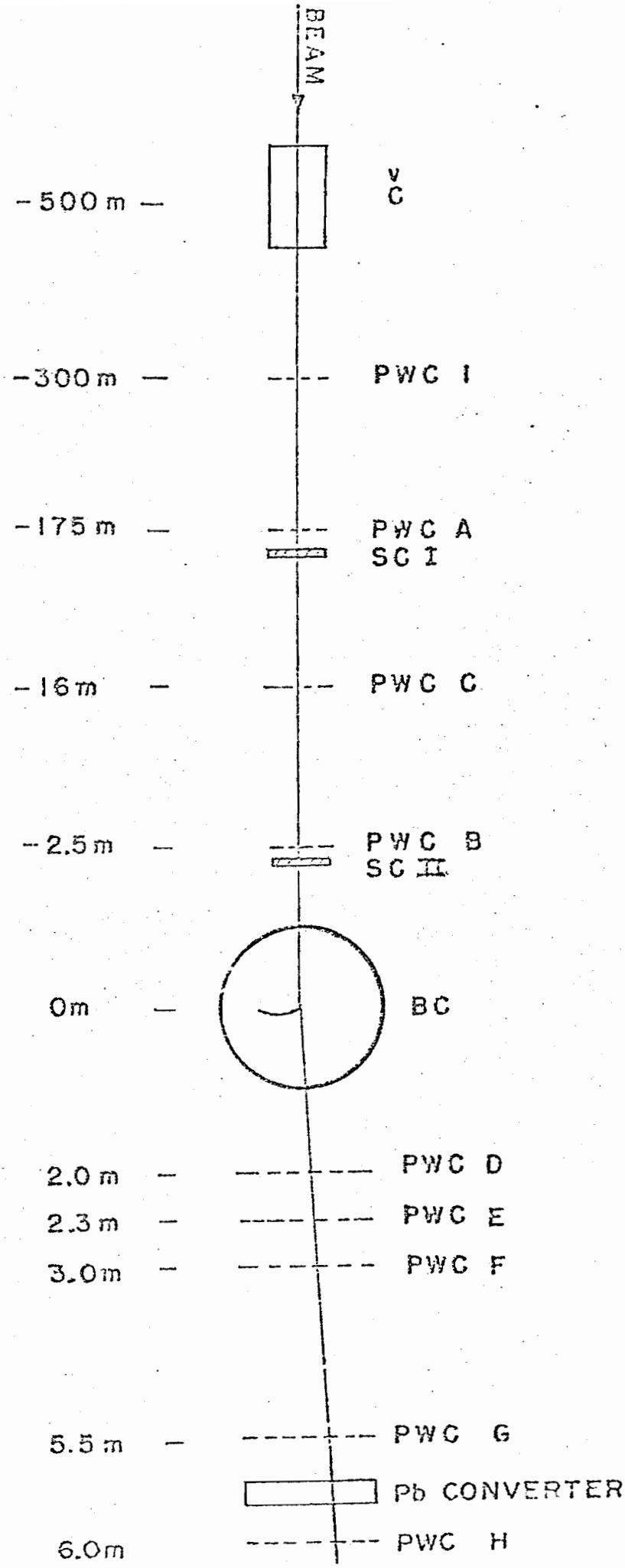
BEAM
-500 m
VC
-300 m
PWC I
-175 m
PWC A
SC I
-16 m
PWC C
-2.5 m
PWC B
SC II
0m
BC
2.0 m
PWC D
2.3 m
PWC E
3.0m
PWC F
5.5 m
PWC G
Pb CONVERTER
6.0m
PWC H

Fig. 1

Fig. 2

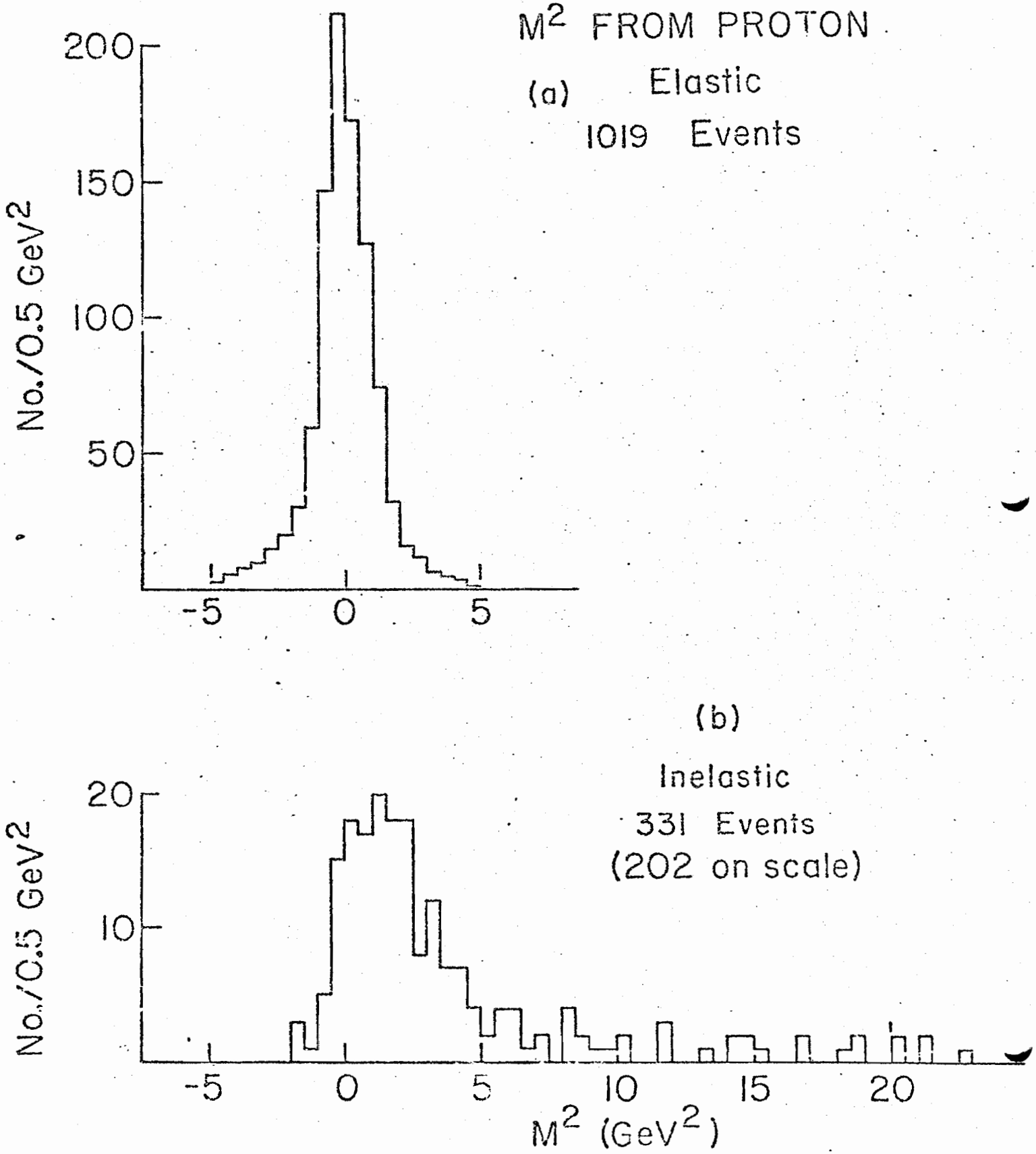
M2 FROM PROTON
(a)
Elastic
1019 Events
200
150
100
50
No./0.5 GeV2
-5
0
5
(b)
Inelastic
331 Events
(202 on scale)
20
10
No./0.5 GeV2
-5
0
5
10
15
20
M2 (GeV2)

Fig. 3

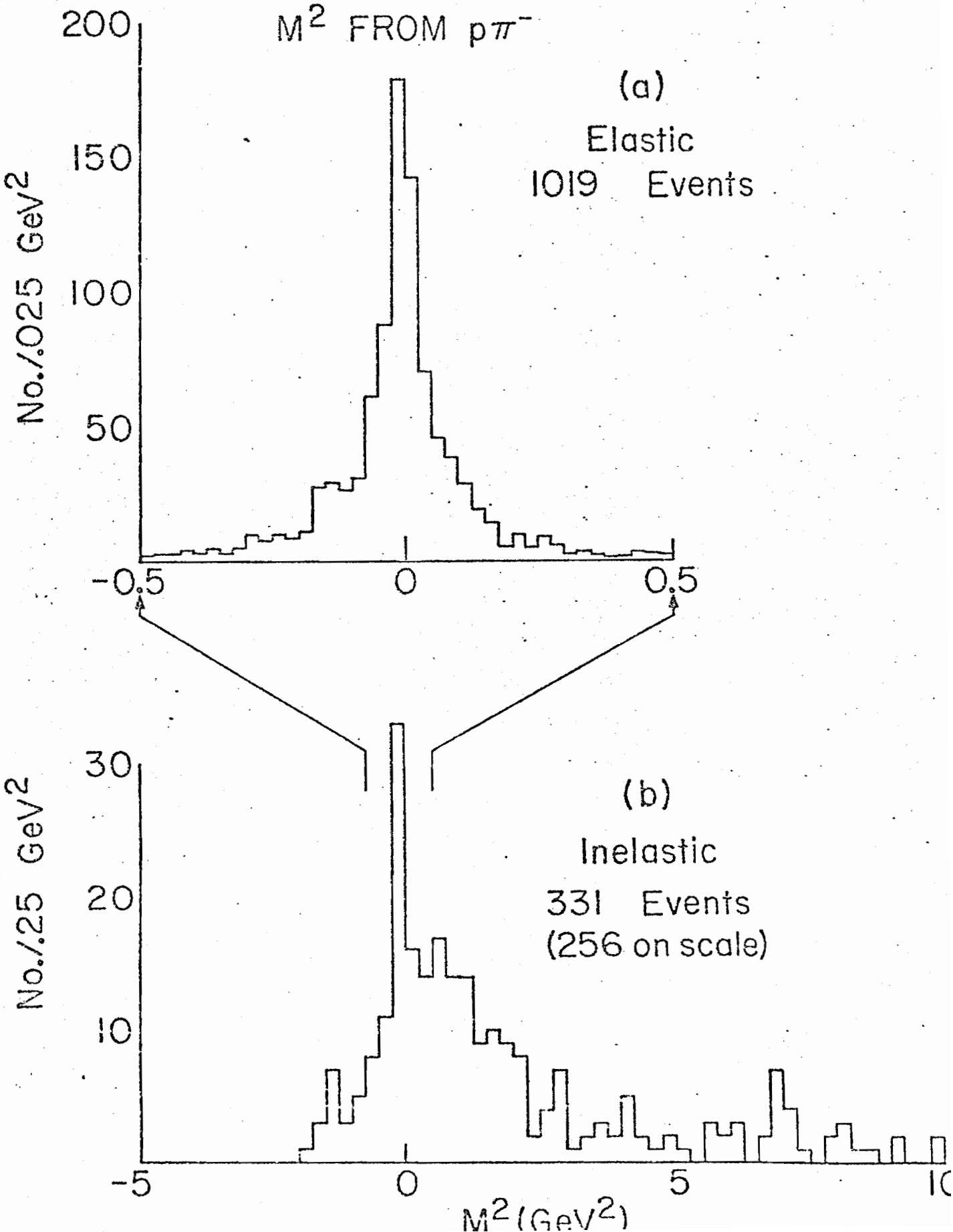
M² FROM pπ⁻
(a)
Elastic
1019 Events
No./.025 GeV²
200
150
100
50
-0.5
0
0.5
(b)
Inelastic
331 Events
(256 on scale)
No./.25 GeV²
30
20
10
-5
0
5
10
M² (GeV²)

147 GeV/c

$\pi^- p \rightarrow \pi^- p$ + neutrals

331 Events

Fig. 4

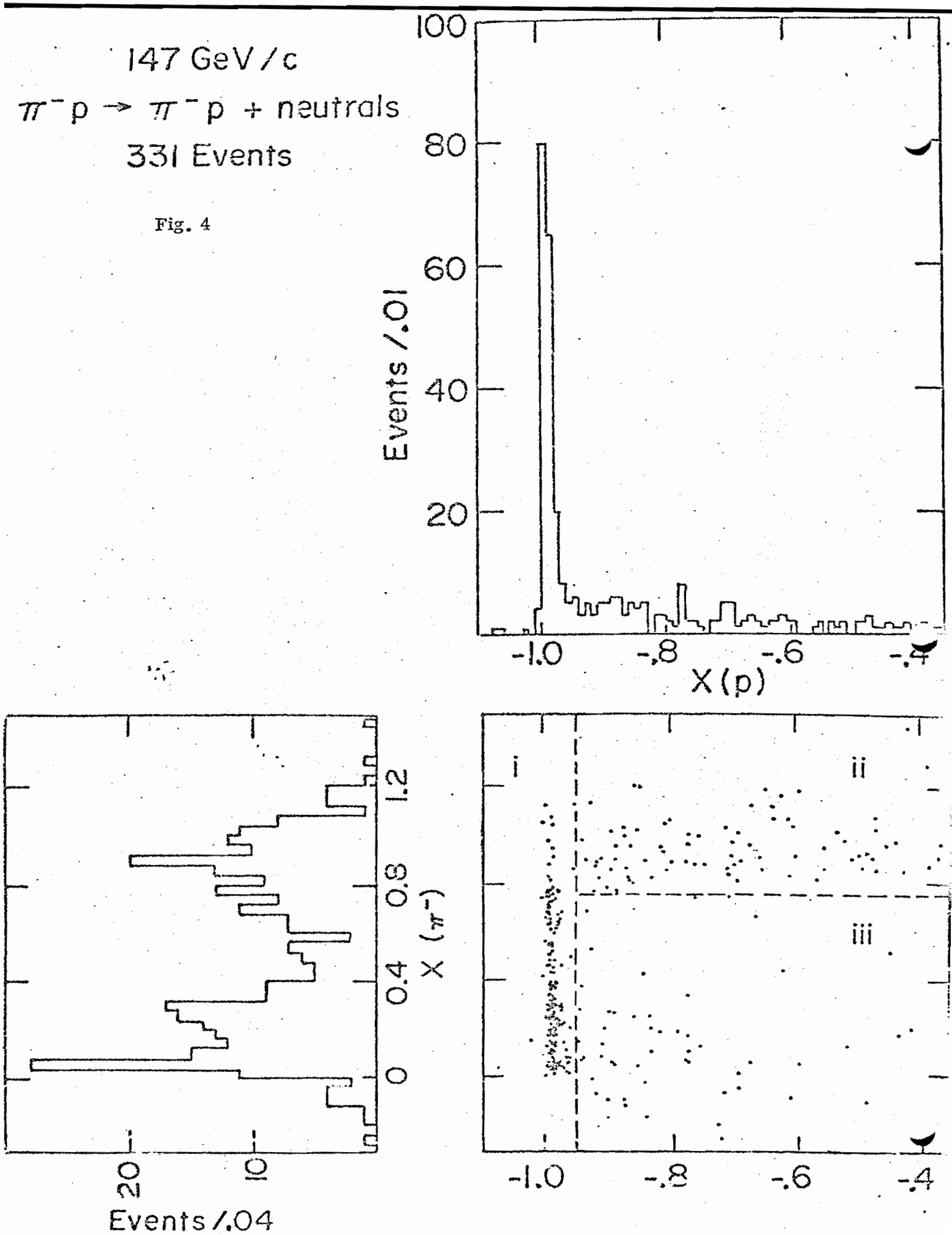

Fig. 5a

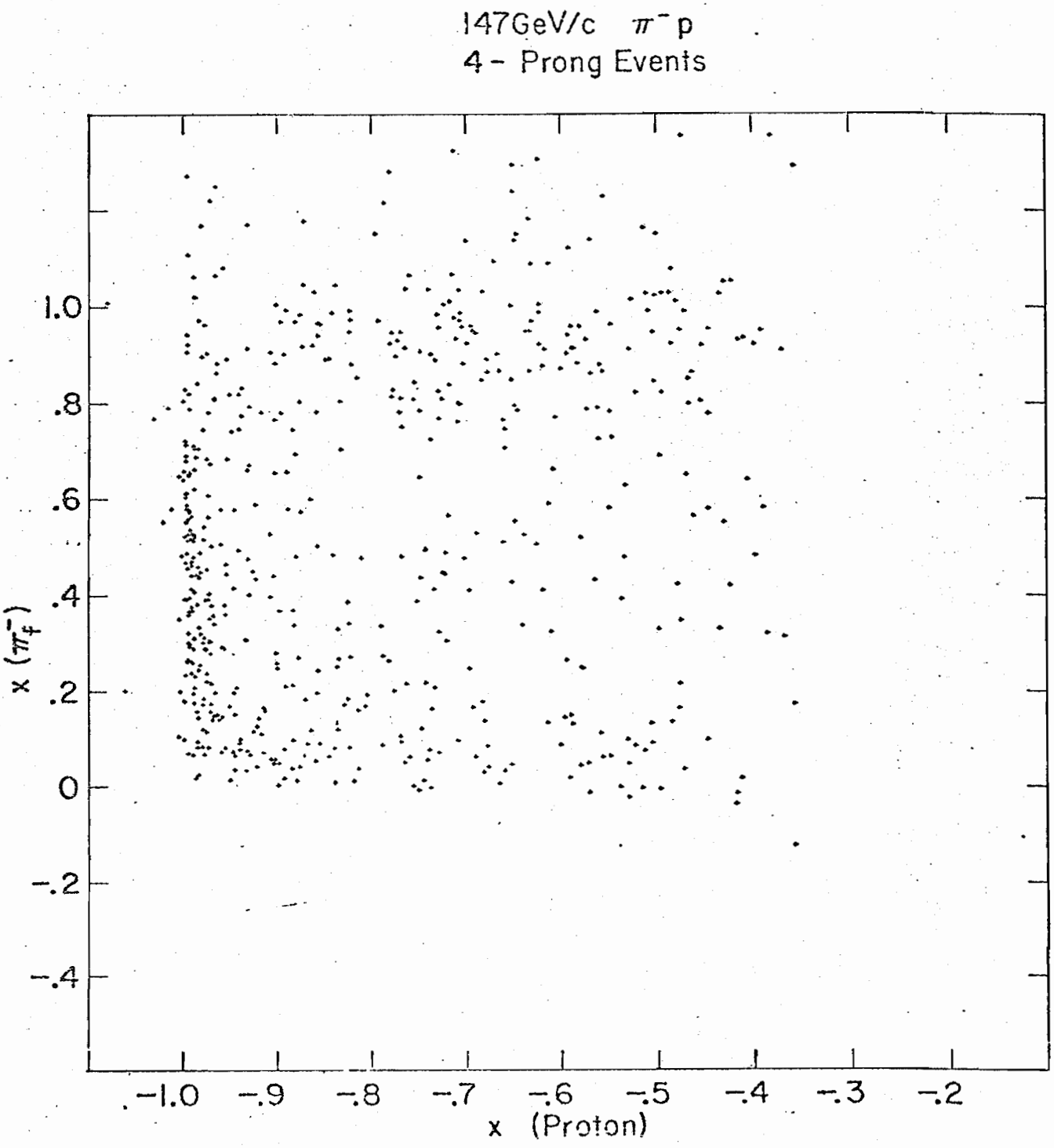
147GeV/c $\pi^- p$
4 - Prong Events
1.0
.8
.6
.4
.2
0
-.2
-.4
x (π_f^-)
-1.0
-.9
-.8
-.7
-.6
-.5
-.4
-.3
-.2
x (Proton)

Fig. 5b

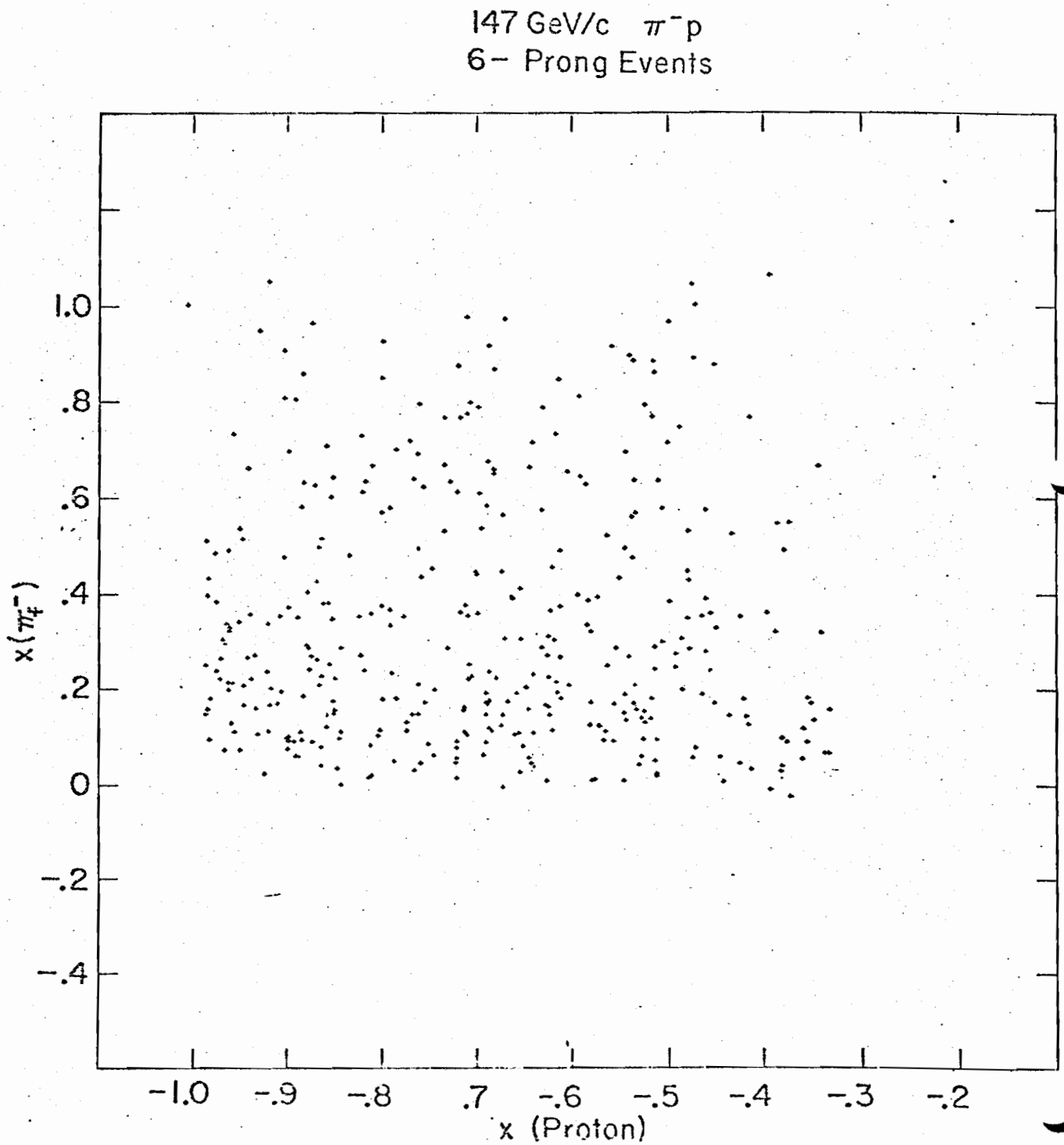
147 GeV/c $\pi^- p$
6- Prong Events
1.0
.8
.6
.4
.2
0
-.2
-.4
$x(\pi_f^-)$
-1.0
-.9
-.8
.7
-.6
-.5
-.4
-.3
-.2
x (Proton)

147 GeV/c

$^-p \rightarrow \pi^-\pi^+$ +neutrals

290 Events

Fig. 6

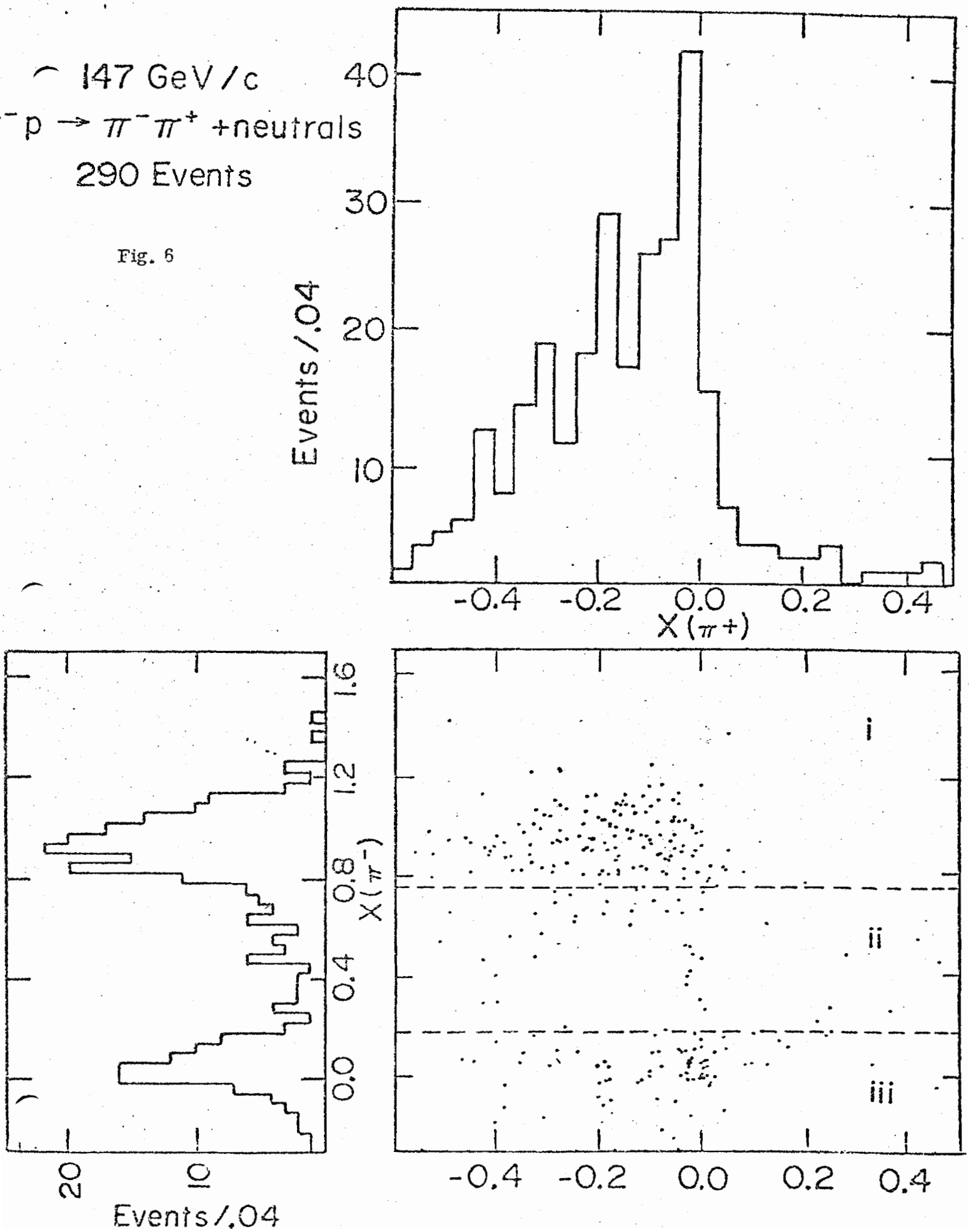

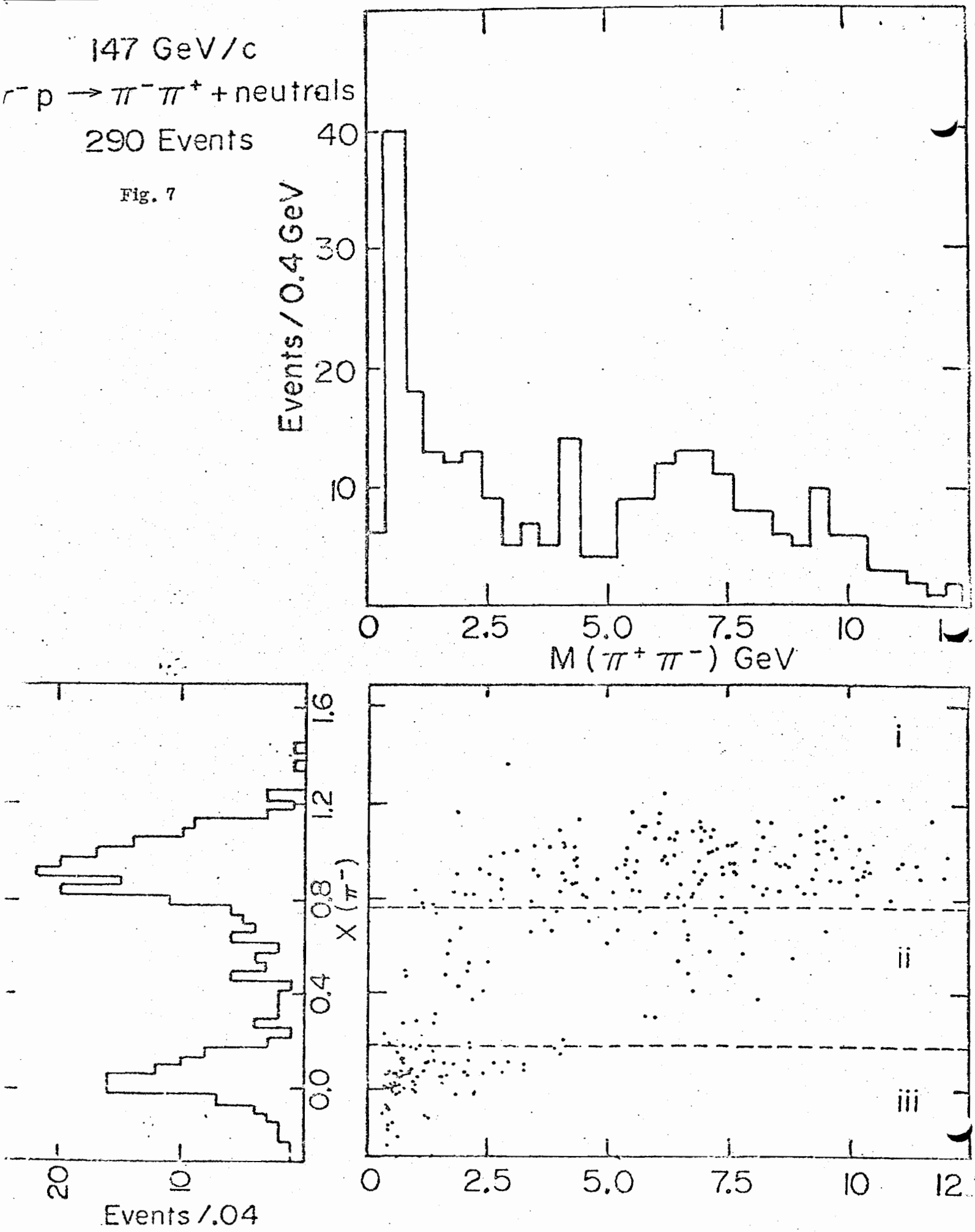
147 GeV/c
$\pi^- p \rightarrow \pi^- \pi^+ +$ neutrals
290 Events
Events / 0.4 GeV
40
30
20
10
0
2.5
5.0
7.5
10
M ($\pi^+ \pi^-$) GeV
1.6
1.2
0.8
0.4
0.0
X (π^-)
i
ii
iii
20
10
Events /.04
0
2.5
5.0
7.5
10
12

Fig. 7

Fig. 8

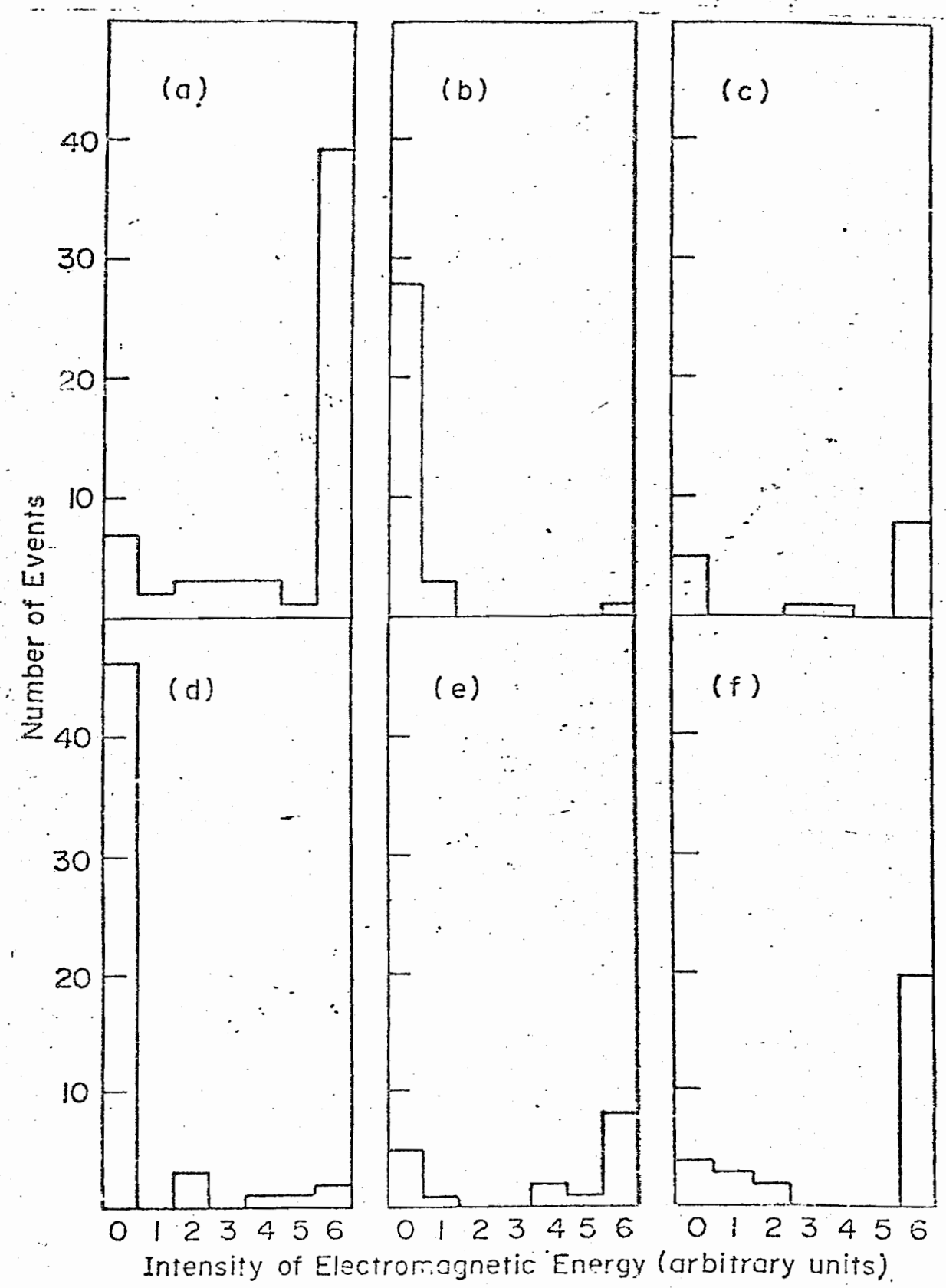
(a)
(b)
(c)
(d)
(e)
(f)
Number of Events
40
30
20
10
0 1 2 3 4 5 6
Intensity of Electromagnetic Energy (arbitrary units)

Fig. 9a

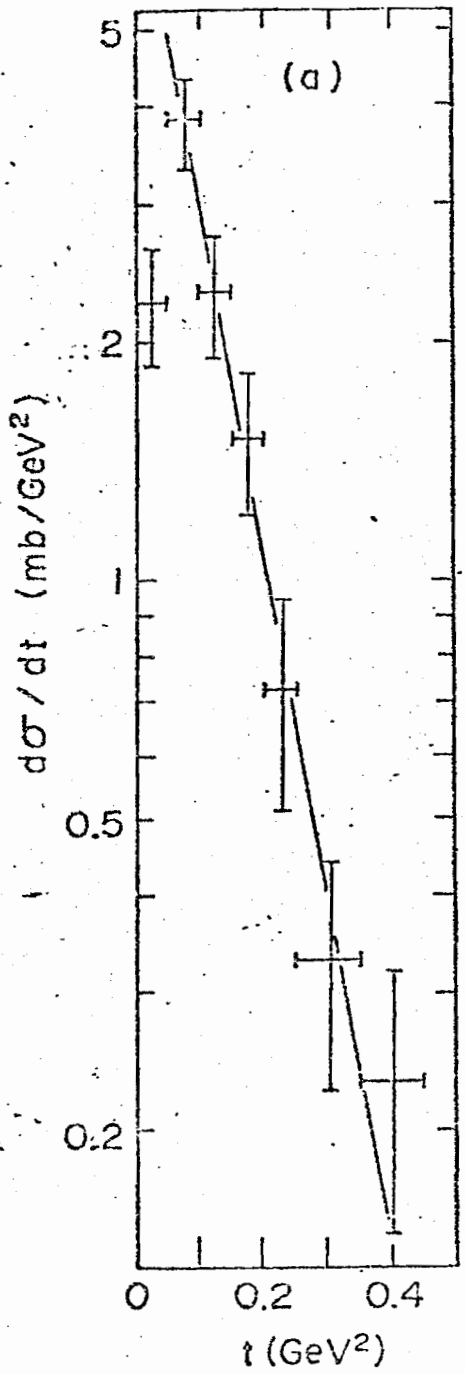

Fig. 9b, c, d

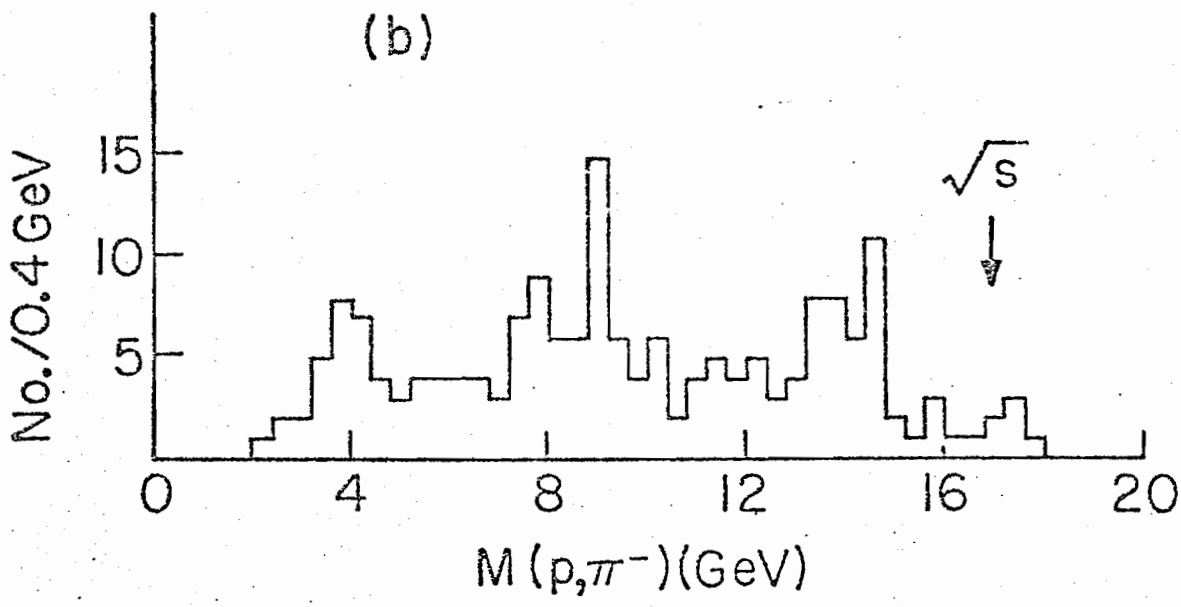
(b)
No./0.4 GeV
15
10
5
0
4
8
12
16
20
√s
M(p,π⁻)(GeV)

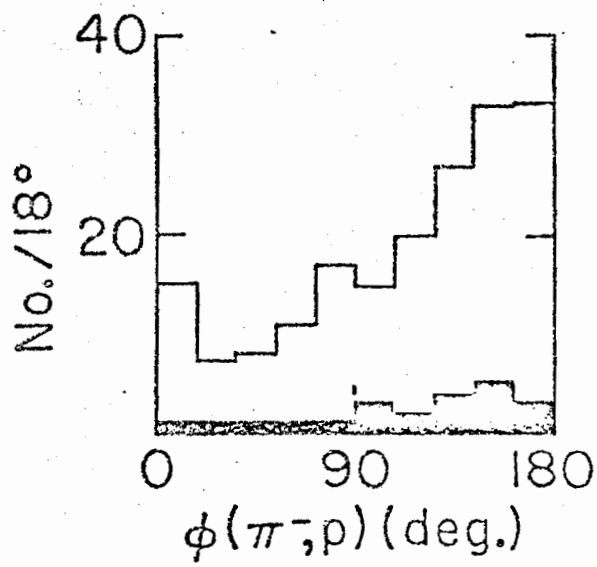
(c)
No./18°
40
20
0
90
180
φ(π⁻,p)(deg.)

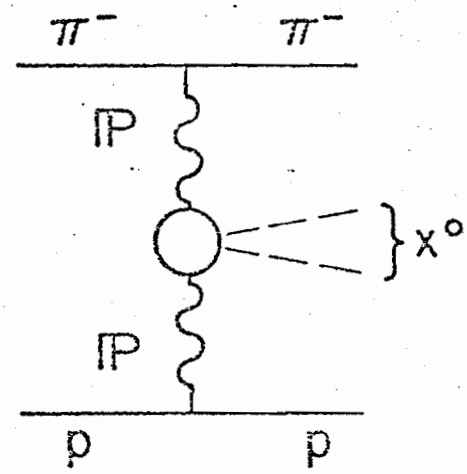
(d)
π⁻
π⁻
IP
IP
x°
p
p

Fig. 10a, b, c

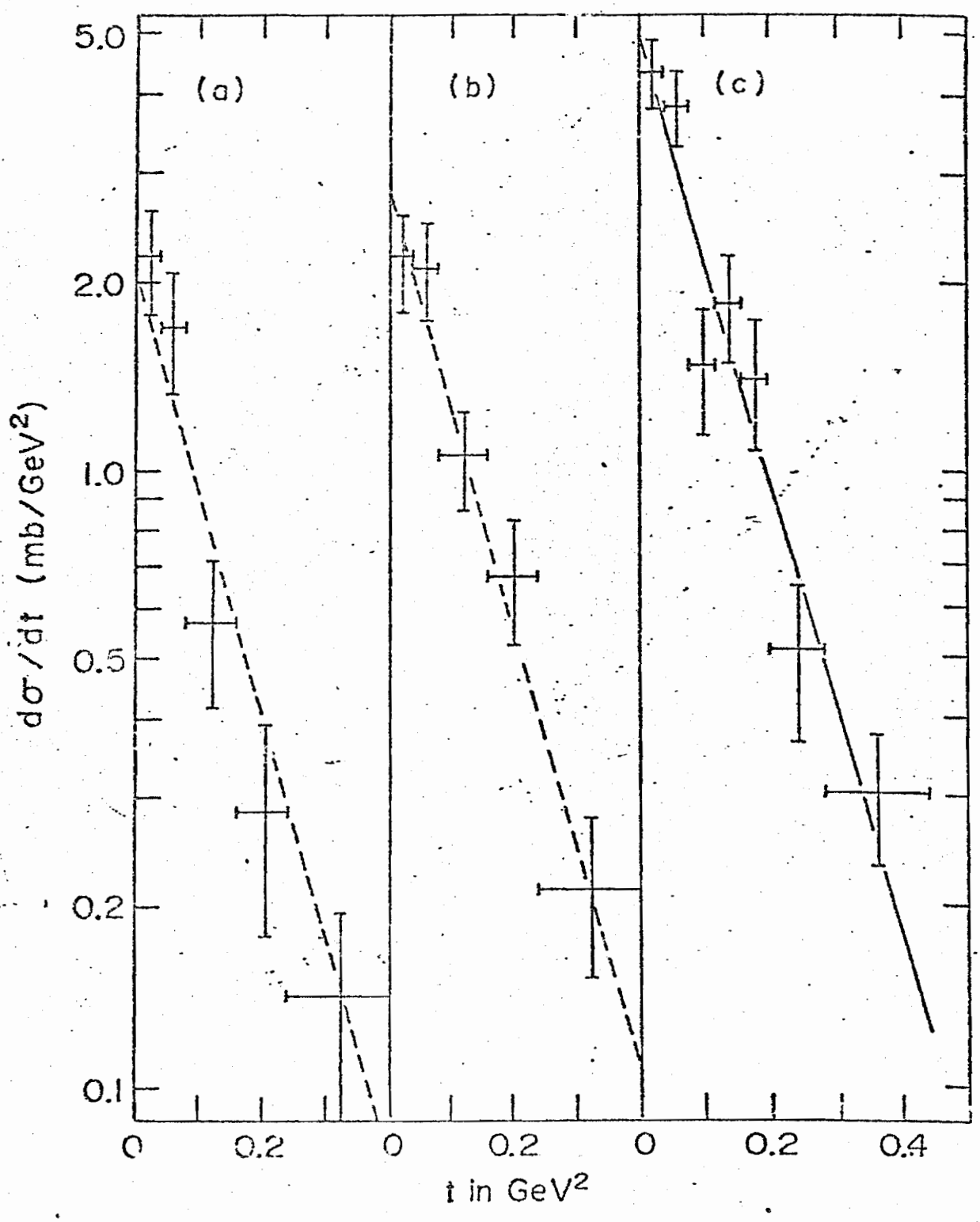

Fig. 10 d, e

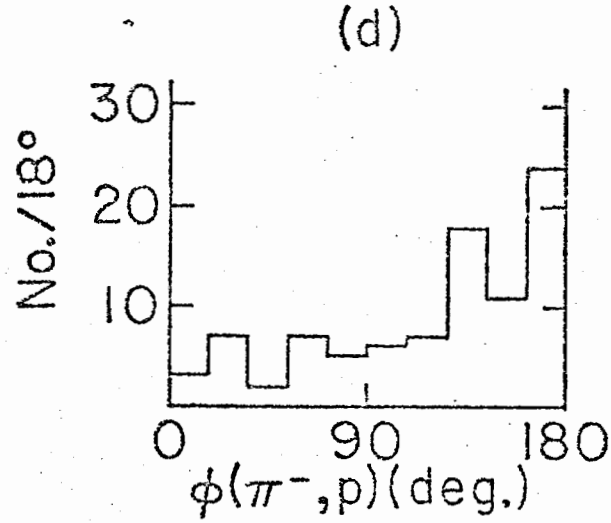

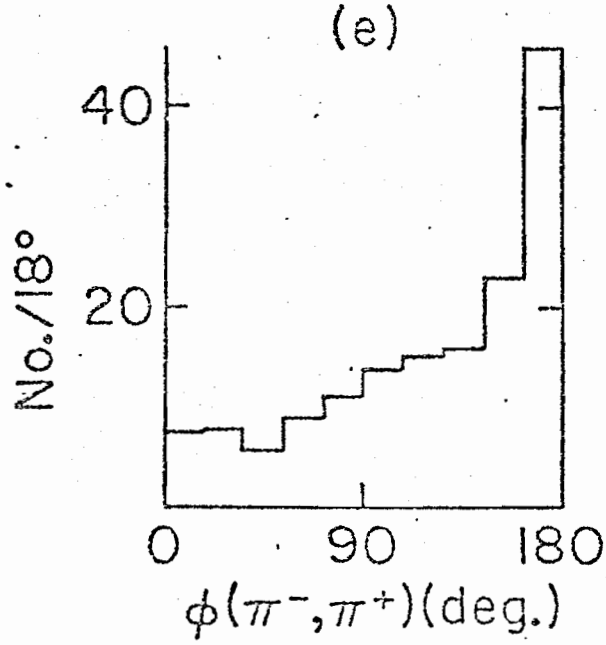

Fig. 11

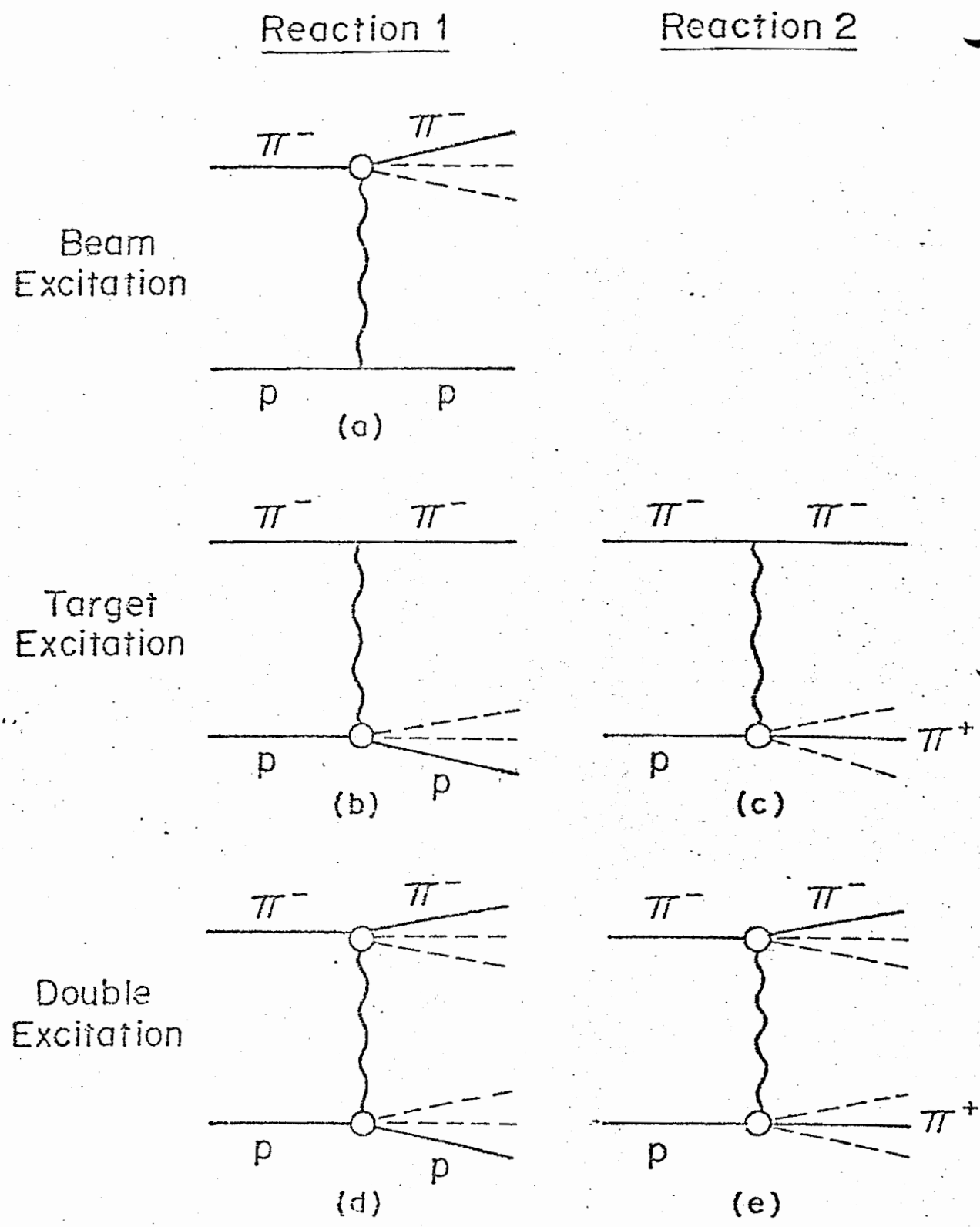
Reaction 1
Reaction 2
Beam Excitation
Target Excitation
Double Excitation
π⁻
π⁺
p
(a)
(b)
(c)
(d)
(e)

Fig. 12

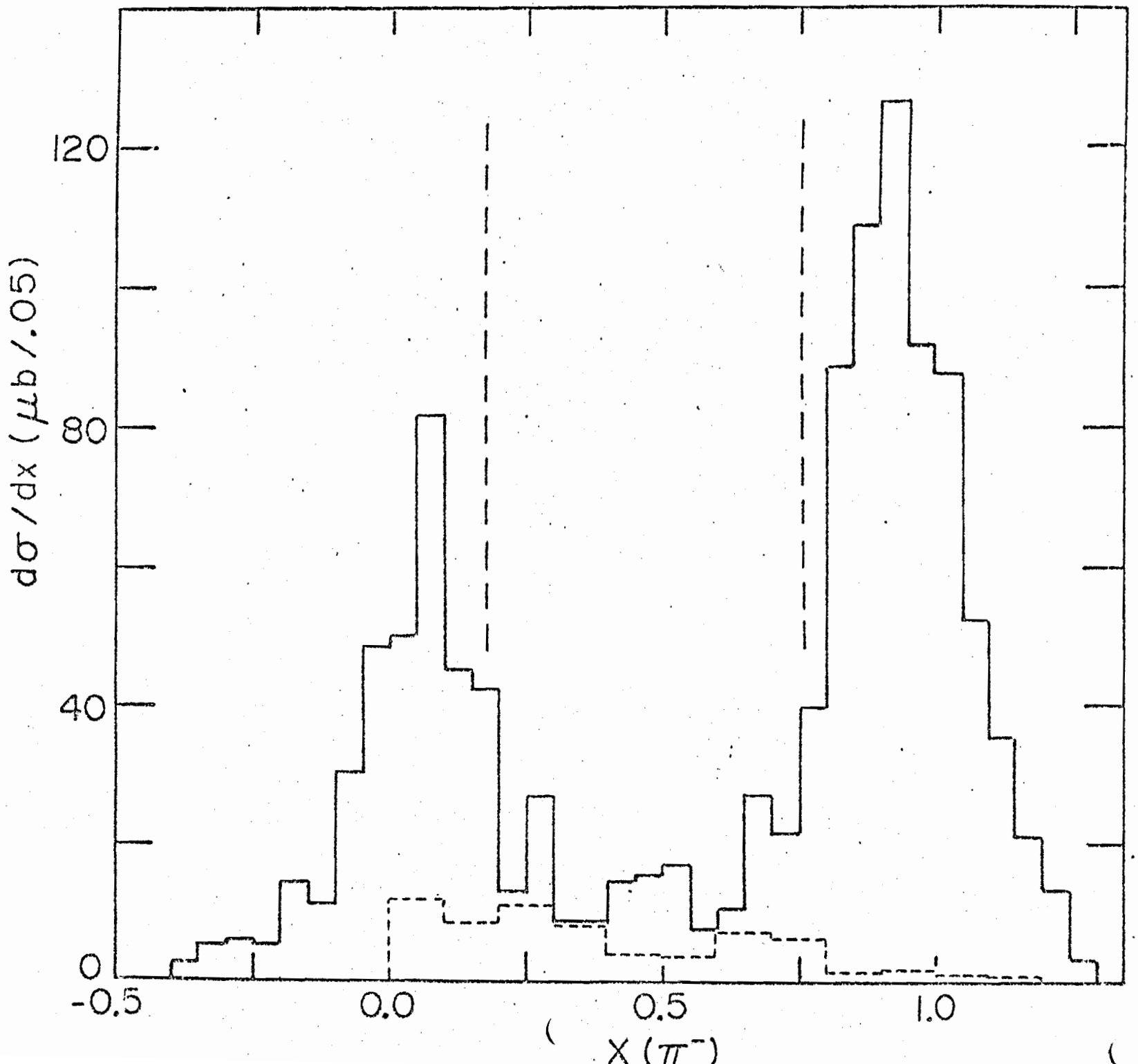

Fig. 13

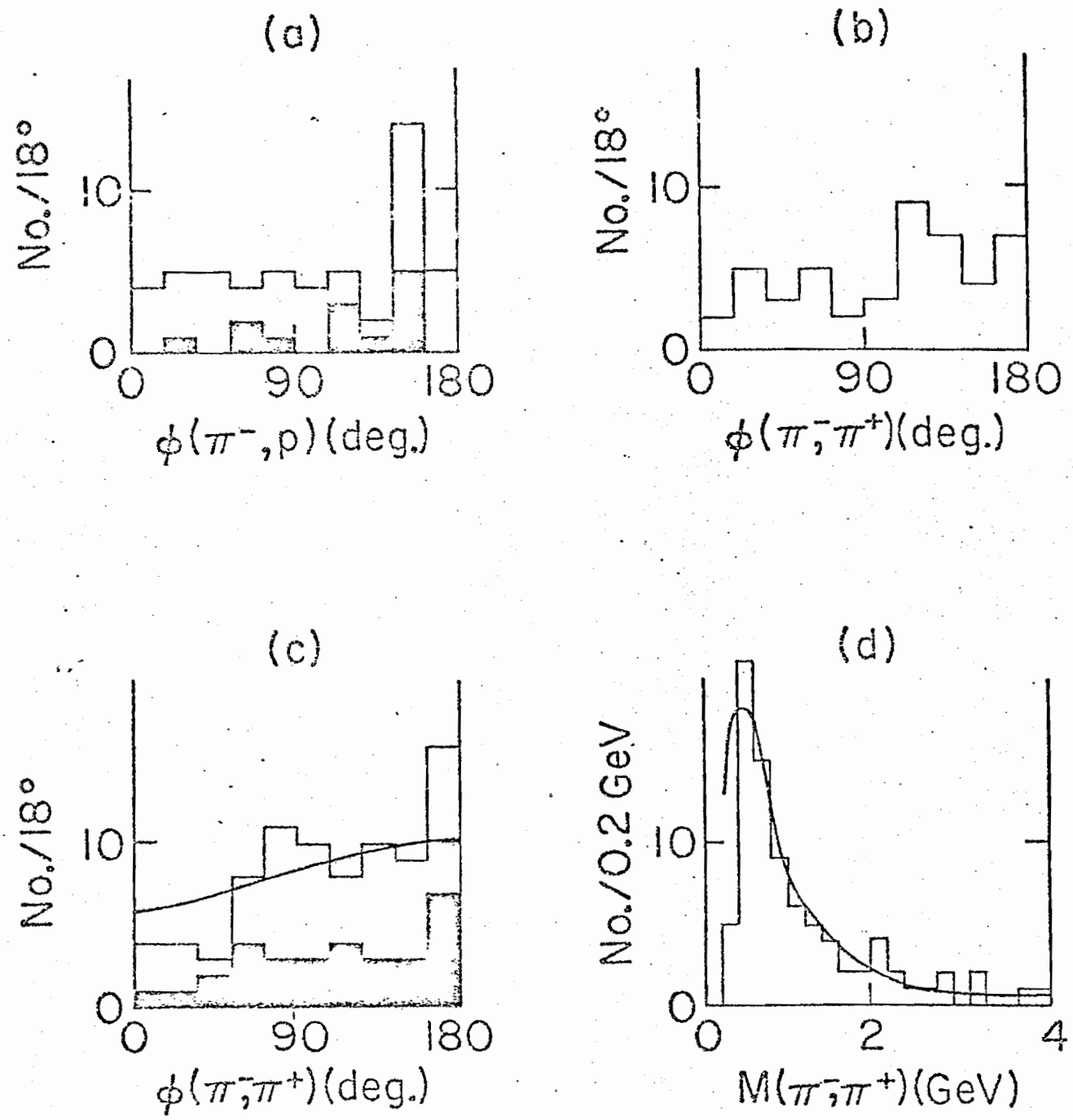
(a)
No./18°
10
0
0
90
180
φ(π⁻,p)(deg.)
(b)
No./18°
10
0
0
90
180
φ(π⁻,π⁺)(deg.)
(c)
No./18°
10
0
0
90
180
φ(π⁻,π⁺)(deg.)
(d)
No./0.2 GeV
10
0
0
2
4
M(π⁻,π⁺)(GeV)